Engineering 5 (2019) 1159–1170

Contents lists available at ScienceDirect

Engineering

journal homepage: www.elsevier.com/locate/eng

Research
4D Printing—Article

Preliminary Investigation of the Reversible 4D Printing of a Dual-Layer Component

Amelia Yilin Lee [a,*], Jia An [a], Chee Kai Chua [a,b,*], Yi Zhang [a]

[a] Singapore Centre for 3D Printing, School of Mechanical and Aerospace Engineering, Nanyang Technological University, Singapore 639798, Singapore
[b] Engineering Product Development, Singapore University of Technology and Design, Singapore 487372, Singapore

ARTICLE INFO

Article history:
Received 31 January 2019
Revised 9 May 2019
Accepted 29 May 2019
Available online 29 September 2019

Keywords:
4D printing
Additive manufacturing
Shape memory polymer
Reversible 4D printing
Two-way 4D printing
Elastomer swelling

ABSTRACT

The rapid development of additive manufacturing and advances in shape memory materials have fueled the progress of four-dimensional (4D) printing. With increasing improvements in design, reversible 4D printing—or two-way 4D printing—has been proven to be feasible. This technology will fully eliminate the need for human interference, as the programming is completely driven by external stimuli, which allows 4D-printed parts to be actuated in multiple cycles. This study proposes a new reversible 4D printing actuation method. The swelling of an elastomer and heat are used in the programming stage, and heat is used in the recovery stage. The main focus of this study is on the self-actuated programming step. To attain control over the bending, a simple predictive model has been developed to study the degree of curvature. The parameters, temperature, and elastomer thickness have also been studied in order to gain a better understanding of how well the model predicts the curvature. This understanding of the curvature will provide a great degree of control over the reversible 4D-printed structure.

1. Introduction

The development of new techniques and materials in the three-dimensional (3D) printing of polymers has fueled the growth of the four-dimensional (4D) printing of polymers [1,2], which is otherwise known as the 3D printing of shape memory polymers (SMPs) [3]. In 4D printing, printed objects can be programmed to carry out shape changes in response to environmental factors [4]. However, 4D printing is still in its early stage of development. In comparison with the conventional manufacturing of SMPs, the 4D printing of polymers still falls behind. One major difference is the lack of reversibility [5]. Reversibility is usually referred to as "two-way memory" because it gives the material two permanent shapes [6]. Most current 4D printing demonstrations require reprogramming after each recovery. Reversibility enables repeated actuation and eliminates the need for reprogramming, which is usually time- and labor-consuming and might lack precision in each reprogramming cycle. Reversibility will allow the use of SMPs in applications with complex geometry and elaborate designs. Fig. 1 depicts the effects of irreversible (one-way) shape memory and reversible (two-way) shape memory with heating and cooling as the stimuli [5].

In recent years, successful breakthroughs have occurred in reversible 4D printing. While the majority of this work has been in the field of hydrogels, there are some examples of polymer composites. Several mechanisms have been utilized to program 4D-printed hydrogels. Naficy et al. [7] developed an extruded hydrogel composite hinge that enables reversible actuation. They used temperature and hydration as the stimuli to carry out shape setting. Su et al. [8] used two different solvents, acetone and water, as the respective stimuli. The printing was carried out in two steps by printing the active areas and passive areas separately. The bending behavior of the printed parts was explained by Timoshenko theory, which involves anisotropic expansion of the bilayer structure. While the above two methods were printed with bio-extrusion, reversible 4D printing was also attempted with digital light printing that offered a faster printing speed. Huang et al. [9] printed a hydrogel with active sections containing ionic potassium 3-sulfopropylmethacrylate (PSPMA) in order to attain larger swelling contrast. Like the abovementioned studies, two solvents were used as the respective stimuli for actuation: 0.1 mol·L^{-1} NaCl and water. A similar test was carried out with a wax-based SMP in order to

* Corresponding authors.
E-mail addresses: ylee057@e.ntu.edu.sg (A.Y. Lee), cheekai_chua@sutd.edu.sg (C.K. Chua).

https://doi.org/10.1016/j.eng.2019.09.007

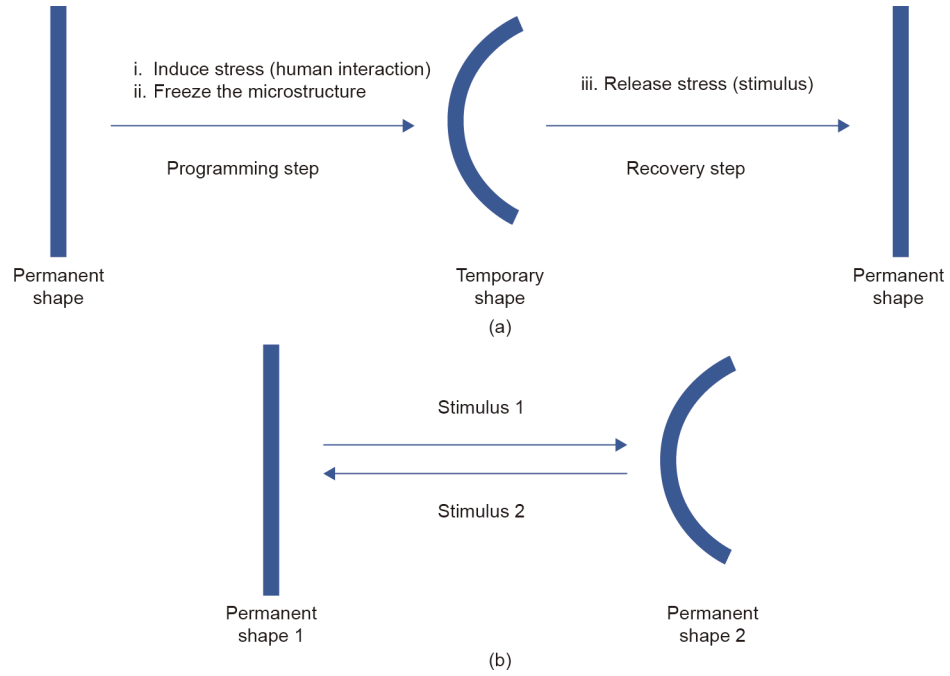

Fig. 1. Process chains of shape memory effects. (a) Irreversible (one-way) shape memory effect; (b) reversible (two-way) shape memory effect.

demonstrate that the concept was feasible in various materials. One of the limitations of this concept is that a hydrogel lacks mechanical strength. Thus, the results of this study are more suitable for biomedical applications and less likely to be used for load-bearing applications.

Other studies have employed materials with stronger mechanical properties, such as the studies by Mao et al. [10] and Ula et al. [11]. Mao et al. utilized the multi-material inkjet printer Objet 260 Connex (Stratasys Ltd., USA) to print three layers, each with a function for actuation in either shape setting or recovery. This composite was able to compensate for the hydrogel's lack of mechanical strength with the strength of the SMP section. However, the strength was still relatively low due to the use of a hydrogel. Ula et al. [11] used a liquid crystal elastomer (LCE), which is known to have reversible shape memory properties. The hinges were printed using Objet 260 Connex, and then DuPont™ ME603 silver ink (silver conductor, DuPont de Nemours, Inc., USA) was directly written onto the elastomeric hinge. Next, the researchers fabricated the LCE with normal curing over the silver ink. When the LCE strips were activated by Joule heating of the conductive wire under a given current, the strip bent. When the current was removed, the strip cooled and straightened. The greatest issue with this study was that the device lost its self-actuation capability due to the use of current.

The programming stage of most shape memory composites requires mechanical loading to induce stress on the SMP in order to achieve shape fixing. A similar concept is used in the present study. However, instead of mechanical loading, an environmental stimulus is used. The difference in this work is that the component only comprises two layers, which is similar to the dual component mechanism (DCM) that is used in one-way shape memory. The DCM usually has two or more components with a hard/soft segment structure or an elastic matrix/transition inclusion [12]. The soft segment or elastic matrix is relatively elastic so that it can store elastic energy during programming. The hard segment is considered to be the transition component, and has a stiffness that changes upon heating. The transition component prevents shape recovery at low temperatures due to its higher stiffness at low temperatures. Reheating the component will soften the transition component to remove the constraints, and the stored elastic energy is activated to return the polymer to its original shape [13]. In DCM, mechanical stress is induced on a composite of matrix and fiber above the glass transition temperature; the composite is then cooled to allow shape fixity. In this study, we used a stimulus—instead of the external mechanical force applied manually that is commonly used in one-way 4D printing—to induce a stress on the shape memory polymer that is similar to that of the fibers in DCM.

In the studies by Mao et al. [10] and Naficy et al. [7], the main function of the hydrogel primarily occurs in the programming step, where it swells and induces stress that results in bending when the component is heated. However, we seek to achieve this swelling by other means. In this study, that function is performed by the elastomeric matrix. Elastomers are generally capable of absorbing a large quantity of organic liquids [14]. In the last two decades, elastomers have been used in the drilling of difficult oil and gas wells [15,16]. Some fluids that have been tested with elastomers include toluene and ethanol [17,18]. Graham's law of effusion states that the lower the molecular weight, the faster the diffusion [19]. Therefore, this law suggests that low molecular alcohol swelling is a plausible solution to attain swelling, although it is important for the structure of the elastomer to have functional groups that attract alcohol groups. Elastomers are loosely crosslinked, and thus have more free volume than other polymers [20]; this aids in the rate of swelling. The elastomer has dual functions in this setup used in this study. In the programming step, it swells and induces internal stress; in the recovery step, it converts the stored potential energy into elastic energy and pulls the component back to the permanent shape. As one less material is used, the number of layers can be reduced to just two. In this work, the stimulus used is ethanol, which is able to swell the elastomer; the swelling of the elastomer component is then utilized to induce stress on the transition material due to strain discrepancy. Once the 3D structure is heated above the glass transition temperature (T_g), the induced stress on the transition material is released to change the shape of the printed parts; this gives rise to the first shape change. While

it is likely that a strain difference may be caused by the mismatch in thermal coefficient, Ding et al. [21] reported that when they heated the bilayer of a transition material and an elastomer for a modest deformation, the thermal strain was less than 1% from room temperature to up to 70 °C. Therefore, thermal strain is assumed to be negligible in this study. Since the recovery step has been widely studied—as it is the same as that in heat-induced one-way shape memory—this paper focuses on the self-actuated programming step. In order to achieve better control of the shape change, the swelling behavior of the elastomer must be understood so that the parameters of the swelling can be controlled. A simple predictive model is developed so that the degree of curvature can be studied. This understanding of the curvature will provide a great degree of control over the reversible 4D-printed structure.

2. Materials and methods

2.1. Materials

All the samples were fabricated using an Objet500 Connex3 polyjet printer (Stratasys, Ltd., USA). In the current printing system, all materials were supplied by Stratasys. The materials used in the present research were based on two materials provided by Stratasys: VeroWhitePlus and TangoBlackPlus (product codes from Stratasys). VeroWhitePlus is a hard and rigid material at room temperature with a glass transition temperature of 58 °C, whereas TangoBlackPlus is soft and rubbery at room temperature with a glass transition temperature of −10 °C [22]. The TangoBlackPlus liquid resin comprises urethane acrylate oligomer, *exo*-1,7,7-trimethylbicyclo[2.2.1]hept-2-yl acrylate, methacrylate oligomer, polyurethane resin, and a photoinitiator. The VeroWhitePlus liquid resin consists of isobornyl acrylate, acrylic monomer, urethane acrylate, epoxy acrylate, acrylic monomer, acrylic oligomer, and a photoinitiator. The solvent used was 99% ethanol, obtained from A.P.C. Chemical Industries, Inc., USA.

2.2. Printing parameters

The materials were printed with an Objet500 Connex3 polyjet printer using the Digital Material mode at a resolution of 300 dpi·in^{-1} (1 in = 2.54 cm) along the *x* and *y* axes. All parts were printed at 100 μm·min^{-1} with a layer thickness of 30 μm and up to 85 μm for the *x and y* axes. The resins were cured by ultraviolet (UV) light within the printer.

2.3. Swelling tests of the elastomer

2.3.1. Linear swelling

Three sets of a thin beam of TangoBlackPlus with the dimensions 2 mm × 2 mm × 5 cm were printed. The beam lengths were measured and recorded with a Vernier caliper; the beams were then soaked in ethanol for 24 h. After the beams were removed from the ethanol, the final length of the thin beam was measured and recorded with a Vernier caliper.

2.3.2. Volumetric swelling

Two sets of different shapes were printed of TangoBlackPlus and VeroWhitePlus: a cube with sides of 5.84 cm, and a block with the dimensions 5 cm × 5 cm × 8 cm. These dimensions were used to maintain an approximate total volume of 200 cm^3. Two different shapes were used to investigate whether the elastomer also swelled isotopically. The dry mass of the samples was first weighed using a Mettler Toledo XS204 analytical balance and recorded as m_d. The samples were then placed in ethanol for 24 h at temperatures of 25, 30, 40, 50, and 60 °C. The samples were removed and weighed again. The wet mass was recorded as m_w. The volume was calculated using the formula $v = \alpha(m_d - m_w)/(\rho_o - \rho_l)$, where $\alpha = 0.99985$, ρ_l is the density of the liquid substance, and ρ_o is the density of air [23].

2.4. Tensile test of VeroWhitePlus and TangoBlackPlus

Both materials—that is, VeroWhitePlus and TangoBlackPlus—were tested with the Shimadzu Universal Tester AGS-X series at 10 kN with the test structure compliant with ASTM D638 and ASTM D412, respectively. The samples were loaded at 10 mm·min^{-1}. Both materials were tested at 25 and 60 °C with three replicates. The samples were stabilized at the temperature for 30 min before tensile testing was carried out.

2.5. Reversibility cycle

The reversibility of the bilayer was achieved by two stimuli—ethanol and heat—in the programming stage to cause a shape change from permanent shape 1 to permanent shape 2, as shown in Fig. 2. Then, in the recovery stage, heat stimulus was applied to enable a shape change from permanent shape 2 back to permanent shape 1. A dual-layered strip measuring 4 cm by 1 cm with a thickness of 1.5 mm of TangoBlackPlus and 1.5 mm of VeroWhitePlus was printed. The strip was placed in a beaker of ethanol within a water bath at 25 °C for 1 h. The elastomeric material

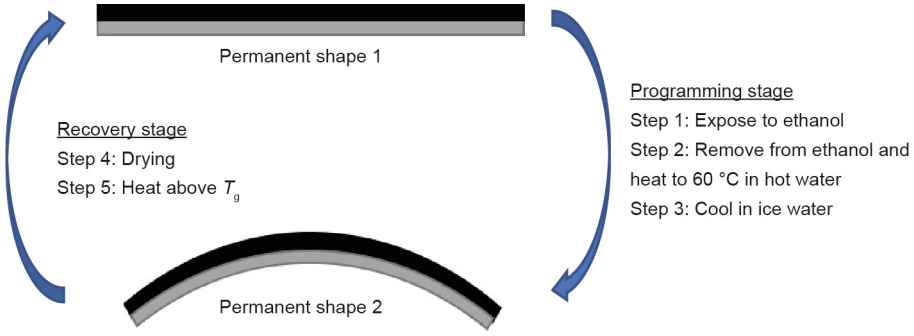

Fig. 2. The two main stages of the reversible cycle: programming and recovery. In the programming stage, there are three steps. Step 1: The first permanent shape is exposed to ethanol. Step 2: The component is removed from ethanol and heated at 60 °C in water to allow the second permanent shape to form. Step 3: The component is cooled to allow the component to fix in the second permanent shape. In the recovery stage, there are two steps. Step 4: The component is left to dry. Step 5: The component is heated to recover to the first permanent shape.

(TangoBlackPlus) swelled and increased in volume. Stress built up as the transition material (VeroWhitePlus) did not swell. The strip was then removed to stop the swelling and placed in another water bath at 60 °C for 5 min. The strip was then removed and placed in ice water for approximately 1 min. The strip was left to dry for 3 h in order to remove the ethanol within the elastomer. To carry out the recovery step, the strip was once again placed in the 60 °C water bath.

2.6. Curvature of bilayer strip

2.6.1. Predictive mathematical model

Because the recovery step, which lasts from Step 4 to Step 5 (Fig. 2), has been widely studied in one-way 4D printing actuated by heat, our focus is on the shape-setting step, which comprises Steps 1 and 2. A model is essential to predict the curvature that can be obtained in shape setting.

A predictive mathematical model was obtained by improvising on the Flory–Rehner equation, the Peppas model, and the mechanics of composites. The swelling of the elastomer can be described and predicted with the Peppas model. The swelling rate of the equilibrium is determined by the Flory–Rehner equation [24].

$$\ln(1-v_2)+v_2+\chi v_2^2=-\frac{\rho V_1}{M_c}v_2^{1/3} \tag{1}$$

where v_2 is the polymer volume fraction, χ is the Flory–Huggins interaction parameter, ρ is the density of the polymer, V_1 is the molar volume of the solvent, and M_c is the mean molecular weight of the chains between each successive crosslink.

From the Flory–Rehner equation, the polymer volume fraction v_2 can be found. The equilibrium volume is given as follows:

$$\frac{V_\infty}{V}=\frac{1}{v_2} \tag{2}$$

where V is the dry volume of the elastomer and V_∞ is the equilibrium volume of the swollen elastomer.

The swelling content S_∞, which is also known as the ratio of swelling agent to the dry volume of elastomer, is found using the following equation:

$$S_\infty=\frac{V_\infty-V}{V} \tag{3}$$

To determine the swelling content at various time points, two models are used separately, as each has its own limitations. For short diffusion times, where the fraction of swelling content $S_t/S_\infty<0.6$, the Peppas model will be used. This model is described by a power law:

$$S_t/S_\infty=kt^n \tag{4}$$

where S_t is the swelling content at time t, k is a constant that changes according to the network and geometric structure, and n is the diffusion exponential of the solvent. The constants can be obtained by solving Fick's second law of diffusion [25], which is given as follows:

$$\frac{\partial c}{\partial t}=\frac{\partial}{\partial x}\left(\frac{\partial c}{\partial x}\right) \tag{5}$$

where c is the concentration of the solvent and x is the distance (Fig. 3).

For diffusion into a slab of thickness $2h$, the concentration c_t at any point within the film at time t can be found by the following:

$$\frac{c_t}{c_\infty}=1-\frac{4}{\pi}\sum_{n=0}^{\infty}\frac{(-1)^n}{2n+1}\exp\left[\frac{-D(2n+1)^2\pi^2t}{4h^2}\right]\times\cos\left[\frac{(2n+1)\pi x}{2h}\right] \tag{6}$$

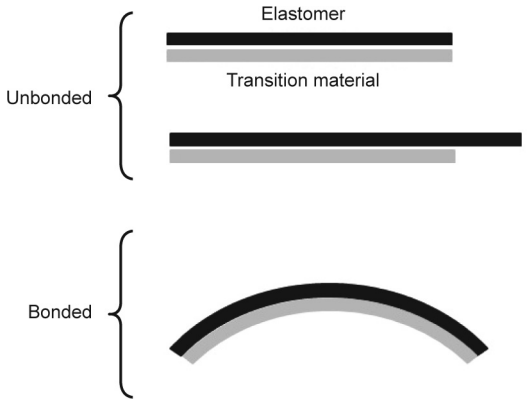

Fig. 3. Illustration of the effects of elongation of the elastomer when unbonded and bonded to the transition material. When bonded, the mismatch in strain results in curvature.

By integrating Eq. (6), the following equation can be obtained:

$$\frac{M_t}{M_\infty}=1-\sum_{n=0}^{\infty}\frac{8}{(2n+1)^2\pi^2}\exp\left[\frac{-D(2n+1)^2\pi^2t}{4h^2}\right] \tag{7}$$

where M_t is the molecular weight at time t and M_∞ is the equilibrium molecular weight.

For short times, Eq. (7) is reduced to be somewhat similar to the Peppas model [26] in Eq. (4),

$$\frac{M_t}{M_\infty}=\frac{2}{h}\left(\frac{D}{\pi}\right)^n t^n \tag{8}$$

Therefore, the constant k is $2(D/\pi)_n/\mathrm{h}$.

The mass diffusivity D is governed by an exponential equation that is temperature T dependent:

$$D=D_0\exp\left(-\frac{E_a}{RT}\right) \tag{9}$$

where D_0 is the maximal diffusion coefficient and E_a is the activation energy for diffusion.

Combining Eq. (9) with Peppas' model, the following equations are obtained:

$$\frac{S_t}{S_\infty}=\frac{2}{h}\left[\frac{D_0t}{\pi}\exp\left(\frac{E_a}{RT}\right)\right]^n \tag{10}$$

For the 4D-printed component, the swellable elastomer on only one side of the slab allows solvent to diffuse in; therefore, the whole equation is divided by two for the component.

$$\frac{S_t}{S_\infty}=\frac{1}{h_e}\left[\frac{D_0t}{\pi}\exp\left(\frac{E_a}{RT}\right)\right]^n \tag{11}$$

where h_e is the thickness of the elastomer.

To find the swelling content that is present in the elastomer at a given time, temperature, and thickness, the following equation is used:

$$V_t=S_tV+V \tag{12}$$

where V_t is the volume at time t.

Assuming that the swelling is isotropic, the linear swelling ratio at time t will be

$$\lambda_t=\left(\frac{V_t}{V}\right)^{\frac{1}{3}}=(S_t+1)^{\frac{1}{3}} \tag{13}$$

The strain ε_x will be

$$\varepsilon_x=\lambda_t-1 \tag{14}$$

Therefore,

$$\varepsilon_x = \left\{\frac{S_\infty}{h_e}\left[\frac{D_0 t}{\pi}\exp\left(\frac{E_a}{RT}\right)\right]^n + 1\right\}^{\frac{1}{3}} - 1 \tag{15}$$

Considering that the two layers of transition material and elastomer are not bonded, the swelling of the elastomer will bring about an increase in strain that does not exist for the transition material. When they are bonded, the mismatch in strain will result in stress that will force the transition material to bend. However, the mechanical strength of the transition material is high at room temperature. The bending force that is created is insufficient to cause a large bending (Fig. 3). Therefore, the transition component is heated above its glass transition temperature. Now, the stiffness of the transition material decreases, enabling the component to bend further. This structure is considered to be a dual-layer composite, and the curvature is calculated using the mechanics of composites. The difference in strain due to the difference in thermal expansion coefficient is assumed to be negligible [21].

To simplify the mechanical model, it is assumed that there are two laminates in the model. In the mechanics of a composite, the plane sections normal to the longitudinal axis remain plane and normal during bending. Hence,

$$\varepsilon_x = \frac{(r+z)\phi - r\phi}{r\phi} = \frac{z}{r} \tag{16}$$

where ε_x is the strain along the x axis, r is the radius of curvature of the neutral surface during bending, ϕ is the angle of the bent material, and z is the furthest distance from the neutral surface defined by the xy plane, which is the neutral axis of the bilayer. z is taken to be the furthest distance, as the elastic modulus of the elastomer tends to be much lower than that of the transition material. To determine the neutral axis of the bilayer, it is first necessary to determine the ratio of the elastic modulus of VeroWhitePlus to the elastic modulus of TangoBlackPlus:

$$\text{ratio} = \frac{E_T}{E_e} \tag{17}$$

where E_T is the elastic modulus of the transition material at 60 °C, and E_e is the elastic modulus of the elastomer at 60 °C.

The bilayer is shown in Fig. 4.

The actual area (A_a) of the cross-section is given as follows:

$$A_a = wh \tag{18}$$

Using the smaller elastic modulus as a base, the area of the elastomer (A_e) will be:

$$A_e = w_e h_e \tag{19}$$

Assuming the bending occurred as though it is a homogeneous material, the difference in the elastic modulus is considered and the centroid axis for the transition material must be normalized; hence, it is necessary to factor in the ratio of the elastic modulus of the transition material to the elastic modulus of the elastomer to the area:

$$A_T = w_T h_T \frac{E_T}{E_e} \tag{20}$$

where w and h refer to width and height, respectively. The subscript T and e refer to transition material and elasomer, respectively.

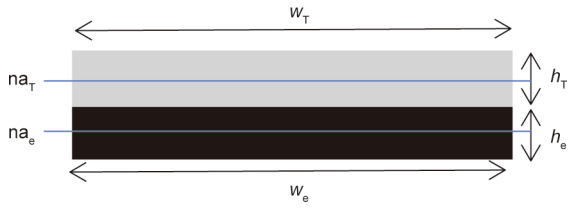

Fig. 4. Height (h) and width (w) of the bilayer.

The neutral axis (na) for the respective materials is as follows:

$$na_T = h_e + \frac{h_T}{2} \tag{21}$$

$$na_e = \frac{h_e}{2} \tag{22}$$

The neutral axis of the bilayer, z, will be:

$$z = \frac{na_T A_T + na_e A_e}{A_T + A_e} \tag{23}$$

$$z = \frac{na_T w_T h_T (E_T/E_e) + na_e w_e h_e}{w_T h_T (E_T/E_e) + w_e h_e} \tag{24}$$

The equation obtained is as follows:

$$\kappa = \frac{1}{z}\left\{\left\{\frac{S_\infty}{h_e}\left[\frac{D_0 t}{\pi}\exp\left(\frac{E_a}{RT}\right)\right]^n + 1\right\}^{\frac{1}{3}} - 1\right\} \tag{25}$$

$$\kappa = \frac{w_T h_T (E_T/E_e) + w_e h_e}{na_T w_T h_T (E_T/E_e) + na_e w_e h_e}\left\{\left\{\frac{S_\infty}{h_e}\left[\frac{D_0 t}{\pi}\exp\left(\frac{E_a}{RT}\right)\right]^n + 1\right\}^{\frac{1}{3}} - 1\right\} \tag{26}$$

where κ is the curvature.

2.6.2. Measurement of curvature

Dual-layer components of TangoBlackPlus and VeroWhitePlus with a length of 4 cm, width of 1 cm, varying thickness of 1.5, 2, 2.5, 3, and 3.5 mm of TangoBlackPlus, and standard thickness of 1.5 mm of VeroWhitePlus were printed and soaked in the four different temperatures of 25, 35, 45, and 55 °C for 60 min. Next, the components were heated to above 60 °C (which is above the T_g of VeroWhitePlus) in water for 1 min to allow the VeroWhitePlus to be heated past its T_g. The components were quickly removed and placed in cold water at 10 °C in order to rapidly cool the component. The samples were then removed and placed on grid paper. The curvatures were determined by measuring the chord length and chord height with a Vernier caliper.

Similarly, dual-layer components of TangoBlackPlus and VeroWhitePlus with a length of 4 cm, width of 1 cm, varying thickness of 1.5, 2, 2.5, 3, and 3.5 mm of VeroWhitePlus, and standard thickness of 1.5 mm of TangoBlackPlus were printed and soaked in the four different temperatures of 25, 35, 45 and 55 °C for 60 min.

The radius is given as follows:

$$R = \frac{d^2 + 4h_c^2}{8h_c} \tag{27}$$

where R is the radius of curvature, h_c is the chord height, and d is the chord length (Fig. 5).

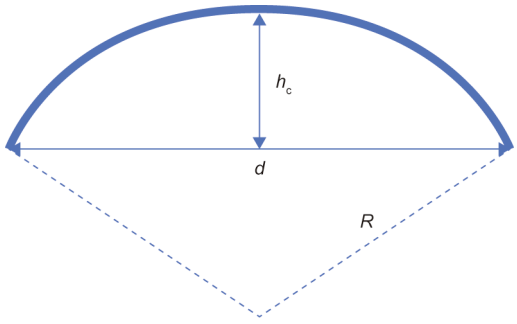

Fig. 5. Measurements of the radius.

The curvature is:

$$\kappa = \frac{1}{R} \tag{28}$$

3. Results and discussion

3.1. Effect of temperature on the swelling of TangoBlackPlus and VeroWhitePlus at equilibrium

The room temperature linear swelling ratio of TangoBlackPlus in ethanol was found to be 1.281, and the volumetric swelling ratio of TangoBlackPlus was found to be 2.102 (Table 1). The linear swelling ratio reached up to 1.652, and the volumetric ratio reached up to 4.506 at 60 °C (Table 1). However, for VeroWhitePlus, the volumetric swelling remained consistently low between 1 and 1.016, which was considered to be negligible. From the equilibrium swelling ratios, the polymer–solvent interaction values were estimated, and the amount of swelling content at equilibrium was obtained. The swelling content indicated the percentage of the volume of ethanol in the elastomer. As shown in Table 1, the amount of swelling content at the equilibrium state increased from 84.28% to 195.5%. Fig. 6 shows that the polymer–solvent interaction values followed a negative power law, which suggests that as the temperature increases further, the change in the interaction value would be less significant than at lower temperatures. This finding suggests that when the average temperature increases, the amount of swelling also increases.

The polymer–solvent interaction parameter is a unitless quantity that functions as an exchange parameter in the lattice model of the polymer solution [27]. The higher the polymer–solvent interaction parameter, the more resistance there is for the solution to enter the polymer matrix, and the less dissolution occurs. In this case, the increase of temperature encourages more mixing of the solvent into the polymer matrix, as the mixing is likely to occur for entropic reasons [28]. As the temperature increases, the affinity between the ethanol and the polymer structure increases. These swelling forces can be converted to the forces required to induce stress on the SMP, the transition material—in this case, VeroWhitePlus. However, it is important to note that the method described here is not the empirical method to obtain the polymer–solvent interaction parameter; rather, it is just an estimate using the Flory–Rehner equation for further study below.

The temperature range for this study lay between the temperatures of 25 and 60 °C. The projected operating temperature should fall within this temperature range. A temperature above 60 °C was not considered, as the solvent is volatile above 60 °C since the boiling point of ethanol is 78.37 °C. This range is particularly desirable because the T_g of VeroWhitePlus is 58 °C [22]. Between 25 and 50 °C, the cycle must be carried out in five separate steps. Between 50 and 60 °C, the cycle can be carried out in four steps, by combining Steps 1 and 2. However, the high-temperature heating of ethanol is not desirable, as the solvent will be constantly in a volatile state.

In addition, it was observed that the TangoBlackPlus tended to degrade after being removed from ethanol at 60 °C after a short period of time. This degradation was likely due to the contraction and diffusion, as well as to the evaporation of the surface ethanol molecules. After the TangoBlackPlus was removed from the heated ethanol, the surface cooled down faster than the core. Therefore, it contracted faster. This situation was exacerbated by the volatility of the ethanol molecules at 60 °C. When the swollen TangoBlackPlus was removed from the ethanol solution, the ethanol molecules near the surface would diffuse out or vaporize faster than the ethanol molecules in the core, resulting in the formation of cracks.

3.2. Tensile results of VeroWhitePlus and TangoBlackPlus

As shown in Table 2 [29,30], the elastic modulus of VeroWhitePlus drops drastically once it is heated past the T_g. The much higher elastic modulus at 25 °C ensures that the bilayer will fix to a rigid structure when cooled. As for TangoBlackPlus, the elastic modulus decreases slightly when heated. This finding suggests that there is little change in the mechanical properties of the TangoBlackPlus.

The general elastic modulus of a hydrogel falls within the range of 1–10 kPa [29], while the combined elastic modulus of a 1:1 ratio

Table 1
Swelling ratios of Tango Black Plus.

Temperature (°C)	Linear swelling ratio	Volumetric swelling ratio	Swelling content at equilibrium
25	1.281	2.102	84.28%
30	1.362	2.527	108.64%
40	1.461	3.121	138.41%
50	1.550	3.722	164.93%
60	1.652	4.506	195.50%

Table 2
Elastic modulus of VeroWhitePlus and TangoBlackPlus at 25 and 60 °C.

Material	Elastic modulus (MPa)	
	25 °C	60 °C
VeroWhitePlus	2136.56	175.0316
TangoBlackPlus	3.0549	2.2462
Hydrogel	1×10^{-3}–1×10^{-4}	—
Grey60	546.235	—

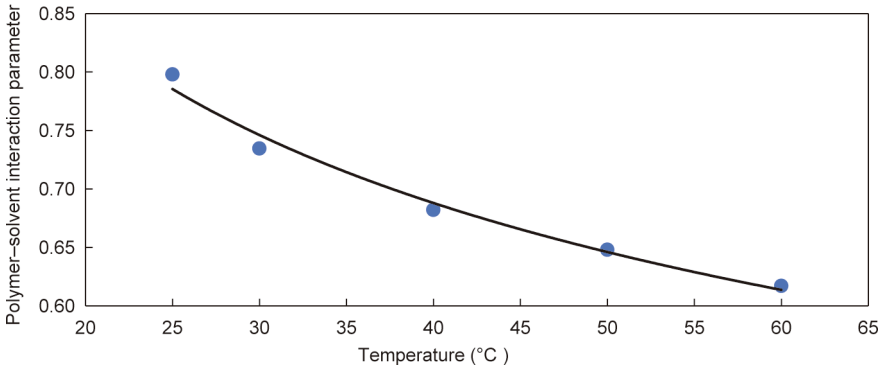

Fig. 6. Graph of the polymer–solvent interaction parameter against temperature.

of our sample has an upper bound elastic modulus of 1070 MPa and a lower bound of 6.101 MPa—at least 600 times higher than that of hydrogels. In the mix that Mao et al. [10] used, which was referred to as Grey60 (also known as DM8530), the SMP layer had a thickness of 0.5 mm, the TangoBlack layer had a thickness of 1.5 mm, and the hydrogel layer had a thickness of 0.5 mm. DM8530 has an elastic modulus of 546.235 MPa, as found by Teoh et al. [30] in a study of the various composites formed by TangoBlackPlus and VeroWhitePlus. The elastic modulus of DM8530 was almost a quarter of that of the original VeroWhitePlus, which will result in lower stiffness. Lower stiffness was also evident in their study, as the mere swelling of the hydrogel before heating was able to cause significant bending.

3.3. Printing design

The working principle of the printing design in this study is similar to that of the DCM in conventional one-way 4D printing. During the programming stage of conventional DCM one-way 4D printing, a mechanical force is usually applied to the printed part when it is heated above the T_g. The part is then cooled so that the transition material can shape set into the temporary shape, as shown in Fig. 1. Elastic energy is stored in the elastomer during the programming stage. This energy will be used in recovery to pull the part back to the original shape when the printed part is heated above the T_g again. Thus, in the programming stage, a force can induced by exerting a stimulus on the bilayer. The programming stage is inspired by the swelling of the hydrogel in the work by Mao et al. [10]. In our case, the swelling occurs in the elastomer instead of the hydrogel.

Similarly to Mao et al., we used multiple materials and multiple stimuli. However, we used a dual layer instead of a triple layer, as shown in Fig. 7. As displayed in Fig. 7, the first layer is an elastomer, and the second layer is a shape-setting polymer. The elastomer replaces the function of the hydrogel in the trilayer component. The swelling of the elastomer elongates the elastomeric section and creates a difference in length. Due to the mismatch in length, the elastomer exerts a force on the shape-setting polymer that was not affected by the solvent. After the shape-setting polymer is heated past the T_g bending occurs, thus enabling self-actuation in the programming stage. By introducing elastomer swelling into the design, the number of layers is reduced to two. The elimination of the hydrogel reduces the materials required to achieve reversible 4D printing. The use of fewer layers and materials simplifies the design and brings convenience to the designer.

In our design, VeroWhitePlus is used as the transition material, as its T_g is 58 °C according to its manufacturer, Stratasys [22]. The high T_g of VeroWhitePlus enables the bilayer to operate at about 60 °C; furthermore, this material is known to have a good recovery rate of about 97% [30].

TangoBlackPlus is used as the elastomeric material, as its T_g is −10 °C according to Stratasys [22]. TangoBlackPlus has a low enough T_g to ensure that it stays rubbery in order to retain elastic energy when the material is cooled down. In addition, the large amount of volumetric swelling (described in Section 3.1) suggests that this is a suitable material to carry out the dual function of exerting stress in the programming stage and storing elastic energy for the recovery stage.

3.4. Demonstration of reversibility

Reversibility was demonstrated using a simple print of the dual flat layers. Fig. 8 shows the feasibility of using a swellable elastomer to achieve the intended shape, shown in the schematic diagram (Fig. 2). In addition, a weight of 1 N was placed on the sample to demonstrate the load-bearing capability when the VeroWhitePlus is cooled back into the glassy state. The VeroWhitePlus in Fig. 8(c) was returned back to its original stiffness.

There are three steps in the programming stage and two steps in the recovery stage of the cycle, as mentioned in Section 2.5 (also see the supplementary video in Appendix A). Step 1 is to immerse the component in ethanol. Ethanol diffuses into the elastomeric section. The overall volume of the elastomeric section increases, as the ethanol molecules are able to diffuse into the free volume and space between chains. However, the internal stress caused by the difference in volume and strain is insufficient to overcome the mechanical stiffness of the transition material at a temperature below the glass transition temperature, as the material is still glassy. Step 2 is to heat the component to above the glass transition temperature of the transition material. This step is carried out to soften the transition material; the mechanical strength of the material will decrease significantly. The internal stress is relieved by the shape change. This shape change forms a second permanent shape. Step 3 is to cool the component. This is a necessary stage, as bringing the temperature to below the glass transition temperature of the transition material will freeze the microstructure of the transition component. The mechanical strength will return to the original state where it is stiff. Step 4 is to allow the component to dry. As the ethanol evaporates and diffuses out of the elastomeric material, the elasticity of the material will return. The volume decreases, and the elastomer will act as a spring pulling the component back into its original shape; however, it is unable to overcome the mechanical strength of the transition material. Hence, elastic potential energy is stored in the elastomeric material. Step 4 is a transition step, as after the first three steps the component can already be at full functionality. Once Step 5 is carried out, heating the material above the glass transition temperature, the transition material softens and decreases in mechanical strength, and the elastic energy of the elastomer pulls it back into the first permanent shape, thus completing a cycle. The whole process takes a total of slightly more than 4 h from programming, to drying, to recovery. This timing suggests that this technique is only suitable for slow actuation.

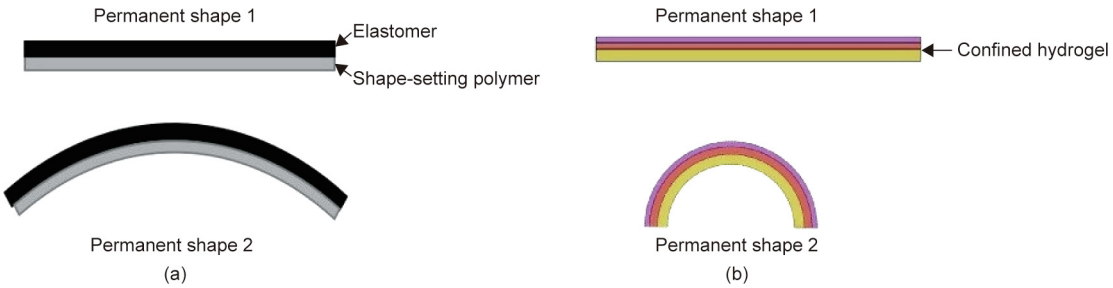

Fig. 7. A comparison of (a) our new design with (b) the existing design.

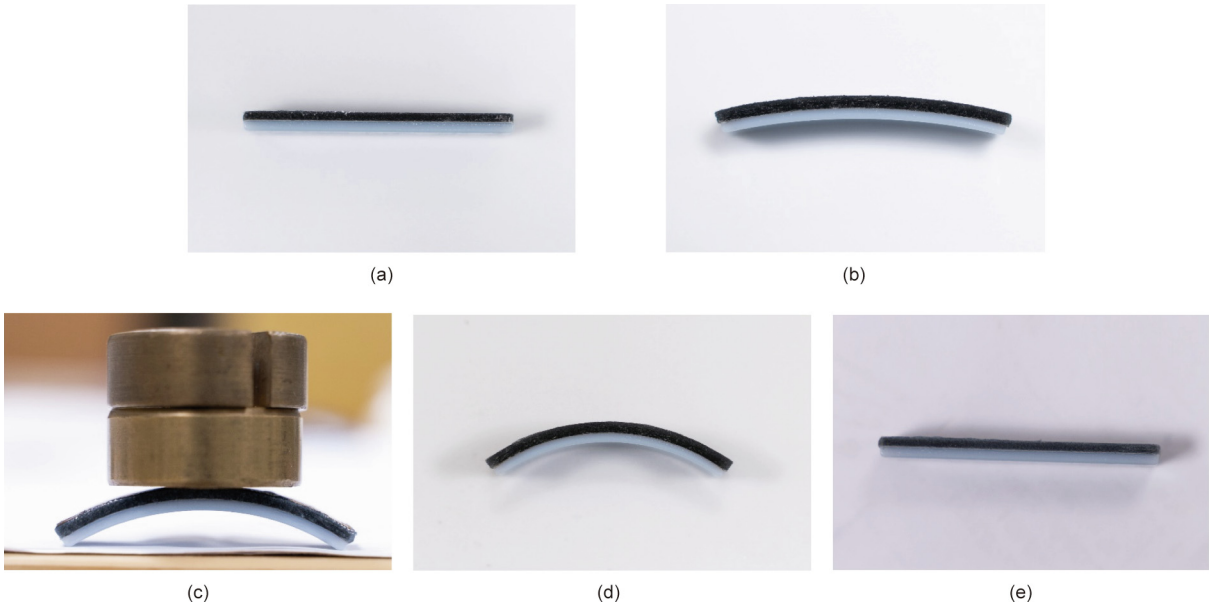

Fig. 8. Experimental samples of the reversible cycle. Programming steps: (a) Side view of original printed sample; (b) side view of sample after being soaked in ethanol at 25 °C for 1 h; (c) side view of sample after it was placed in 60 °C water and then into ice water, and then removed. A 1 N weight is placed on the sample. Recovery steps: (d) Side view of sample left to dry for 3 h; (e) side view of sample after being heated at 60 °C.

3.5. Effect of the thickness of TangoBlackPlus and temperature on curvatures of the dual layer

Using Eq. (25), with the diffusion exponential n found to be 0.6 (Table S1 in Appendix A), the curvature is plotted against the thickness at four different temperature points from 25 to 55 °C, which are the expected operating temperatures of the dual-layer component. A thickness of 1.5–3.5 mm is used in consideration of diffusion. If the thickness is too large, the diffusion will require a longer time, which in turn increases the actuation time. In theory, the smaller the thickness of the elastomer, the larger the curvature. This is shown in Fig. 9 Tables S2 and S3 and is reflected in the experimental results.

The thickness of the TangoBlackPlus plays a large role in the length mismatch. A smaller thickness allows a larger surface-area-to-volume ratio, resulting in a higher percentage of volume of ethanol to volume of elastomer, which gives rise to more bending. With a smaller thickness, the z value decreases too, allowing more bending as described in Eq. (26). The time of swelling is limited to 1 h. It is faster for the ethanol molecules to penetrate and diffuse into the area nearer to the neutral axis for a smaller thickness than for a larger thickness.

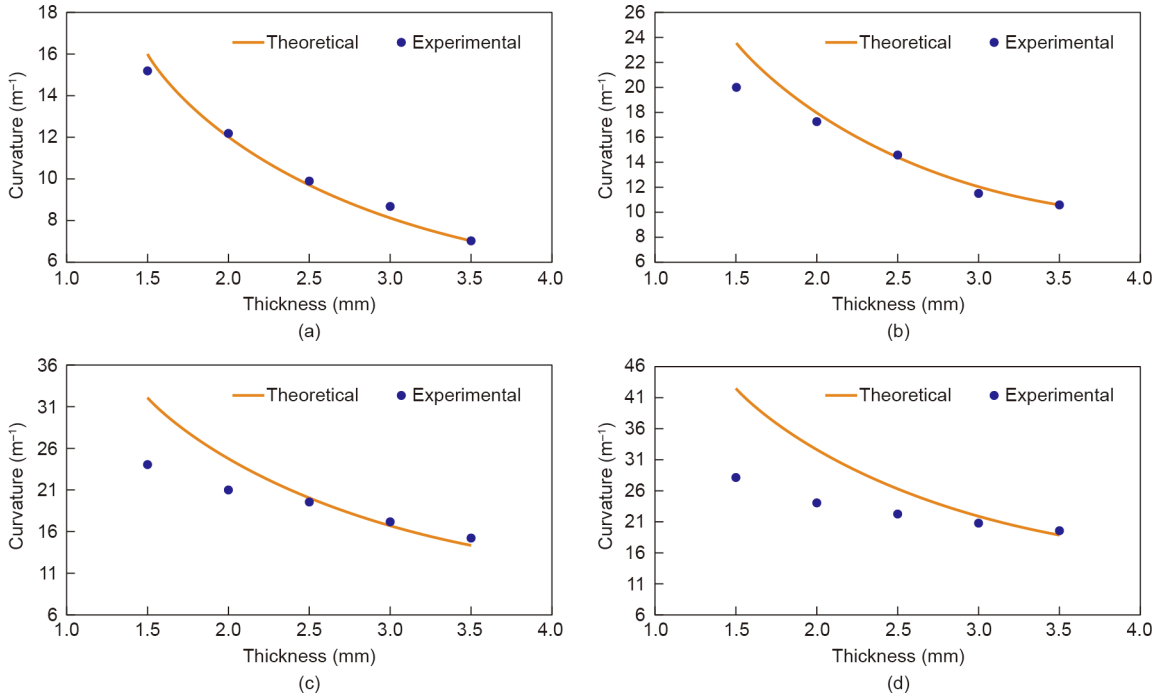

Fig. 9. Graphs of curvature against the thickness of TangoBlackPlus at different temperatures. (a) 25 °C; (b) 35 °C; (c) 45 °C; (d) 55 °C.

The curvatures at each thickness across the temperature range are higher when the temperature is higher. The rate of diffusion increases when the temperature increases. As mentioned earlier, the temperature also affects the affinity between the elastomer and the ethanol.

Both the theoretical and the experimental results show decreasing curvature as the thickness increases. Fig. 9(a) shows that at 25 °C for every thickness, the theoretical model and experimental results are very close. The average degree of discrepancy is 5.78% at 25 °C. This result demonstrates that at 25 °C, the model is able to predict the curvature to a high degree of accuracy. At the temperatures from 35 to 55 °C, the results show a larger parity between the theoretical and experimental results at smaller thicknesses (Figs. 9(b–d)). The difference narrows down to almost nothing at about 3 mm for 35 and 45 °C (Figs. 9(b, c)). This intersection occurs at 3.5 mm at 55 °C (Fig. 9(d)). The percentage of parity for increasing temperature increases with an increasing rate from an average of 5.78% at 25 °C to 22.81% at 55 °C (Table S4). Likewise, on average, the model is able to predict the curvatures at a much higher accuracy with increasing thickness, with a difference of 1.89% at 3.5 mm than at 1.5 mm with a difference of 29.63%.

When the thickness is smaller, the surface-area-to-volume ratio of the elastomer is higher. Ethanol diffuses out and evaporates quickly when the dual-layer strip is removed from the ethanol and exposed to the air. The larger the surface-area-to-volume ratio is, the larger the loss of the percentage of ethanol to elastomer will be. Likewise, at a higher temperature, ethanol will be more volatile. Thus, once the dual-layer strip is removed, a significant amount of ethanol will diffuse out of the elastomer and reduce the amount of swelling force.

The increasing parity at a smaller thickness and higher temperature can be due to the percentage of swelling content in the elastomer too. The equation that is used to predict the behavior is based on the Peppas model, which can model up to a swellable content of 60%. At higher temperatures, especially at 55 °C with a thickness of less than 2.5 mm and with soaking for 1 h, the amount of swelling content exceeds 60% and deviates from the Peppas model; hence, the model is not able to predict the curvature accurately at higher temperatures.

3.6. Surface response for curvature

Ideally, the 3D plot (Fig. 10) shows that at a high temperature and with a small thickness, the largest curvature can be obtained.

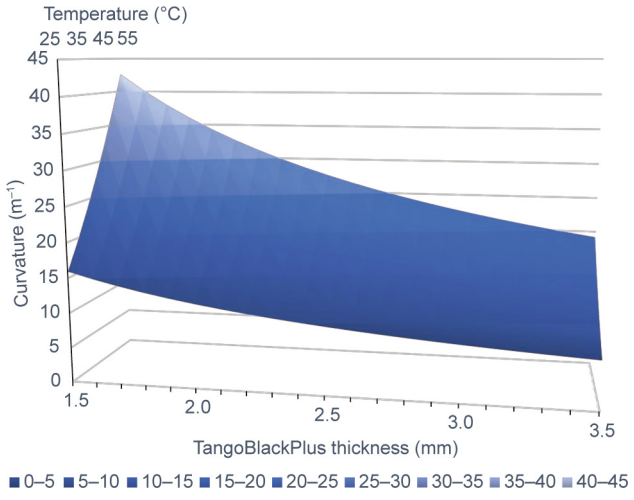

Fig. 10. Surface response graph of the elastomer thickness, swelling temperature, and resultant bilayer curvature.

With a 3D plot, programming of the curvature of the first actuation can be predicted. In addition, the parameters of the actuation can be obtained from the curve.

Although the model is not able to predict as accurately at extremes, within the temperature range of 25–45 °C and for a thickness ranging from 2 to 3.5 mm, the model is still able to predict the curvature to a high degree of accuracy with an average discrepancy of less than 10%. If an extremely small thickness and high temperature are required, a factor might have to be added to account for the difference between the theoretical curvature and the experimental curvature due to the volatility of ethanol.

3.7. Effect of thickness of VeroWhitePlus and temperature on curvatures of the dual layer

Another parameter that will affect the curvature other than swelling is the z value, which is affected by the thickness of both TangoBlackPlus and VeroWhitePlus. The z value will affect the resultant curvature caused by the mismatch in length. The thicker the VeroWhitePlus section is, the stiffer the bilayer will be. The results of the effect of thickness of VeroWhitePlus and temperature on curvatures of the dual layer are shown in Fig. 11.

The experimental results with a VeroWhitePlus thickness between 1.5 and 2.5 mm were close to the theoretical results at all temperatures. This finding suggests that at a smaller thickness when the stiffness is slightly lower, the model can accurately predict the curvatures. However, when the thickness of the VeroWhitePlus increased further, the experimental curvatures fell short of the theoretical curvatures. It was also observed that at a lower temperature, this difference was larger. The large difference between the theoretical and experimental results at 3 and 3.5 mm can be attributed to an inability to attain uniform heating in Step 2, which is limited to 60 s. Therefore, at the end of the 60 s heating, the elastic modulus of the VeroWhitePlus is still high, and the force created by the swelling is unable to induce much curvature, as it is smaller than what is required to create a slight deflection. However, the duration for heating during the programming stage cannot be too long because the ethanol that has entered the elastomer matrix will start to diffuse out once the sample is removed from ethanol and submerged in water. Also, a high temperature will result in a faster diffusion rate out of the TangoBlackPlus, thus reducing the amount of bending and making it difficult to predict the curvature. As the results at 2.5 mm and below produced similar curvatures to the theoretical curvatures, it is safe to consider that the model can make accurate predictions at a VeroWhitePlus thickness of less than 2.5 mm.

3.8. Response rate of the curvature of the dual layer

The response rate of the curvature was also studied for the bilayer with a 1.5 mm thickness of VeroWhitePlus and a 2.5 mm thickness of TangoBlackPlus. These dimensions were used because, as discussed in Section 3.5, these thicknesses show the optimal results of following the theoretical results and having a good amount of curvature at most temperatures. The bilayers were heated at 25 °C for the first 60 min and then heated at 60 °C for the last minute. The curvatures were measured at 1 min intervals when soaked in ethanol and at 1 s intervals during heating; the results were tallied and are shown in Fig. 12. It is shown that during the swelling stage, while there is a very slight curvature, the stiffness of the VeroWhitePlus does not allow the bilayer to bend further. Once the sample is heated at t = 60 min, the bilayer can bend more at an exponential rate.

The curve in Fig. 12 gives an indication of how the first two steps in the programming stage functioned. When soaked in ethanol, the volume of the TangoBlackPlus increased as it swelled up.

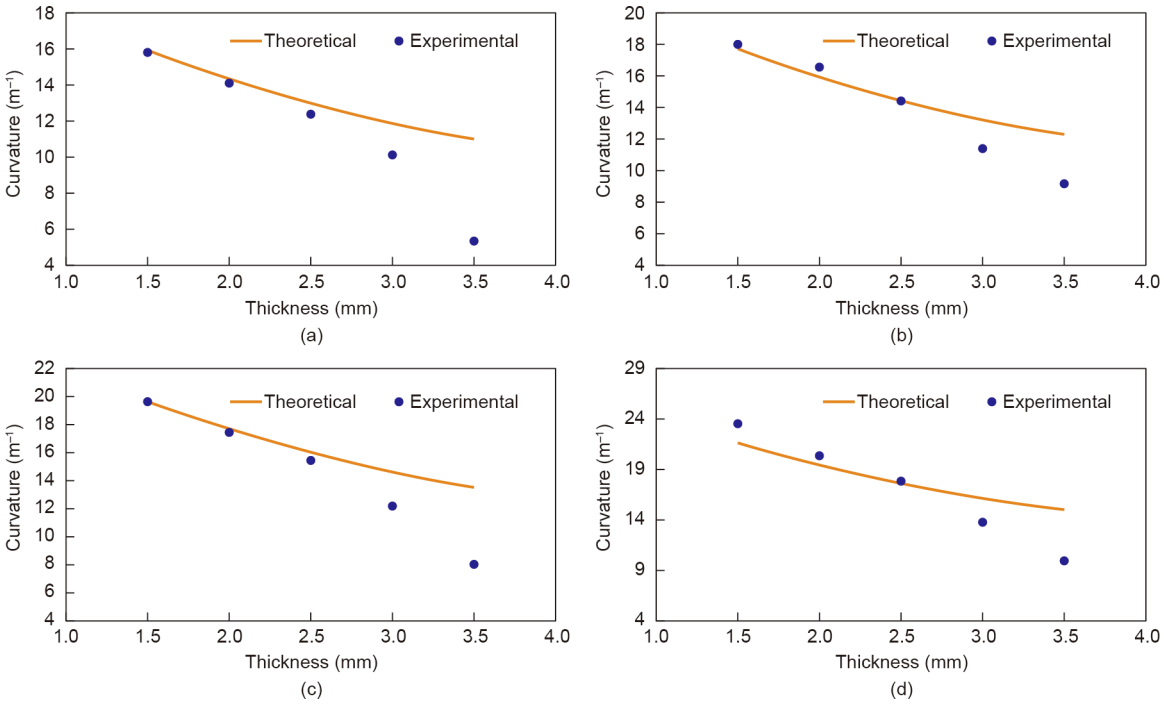

Fig. 11. Graphs of curvature against VeroWhitePlus thickness at different temperatures. (a) 25 °C; (b) 35 °C; (c) 45 °C; (d) 55 °C.

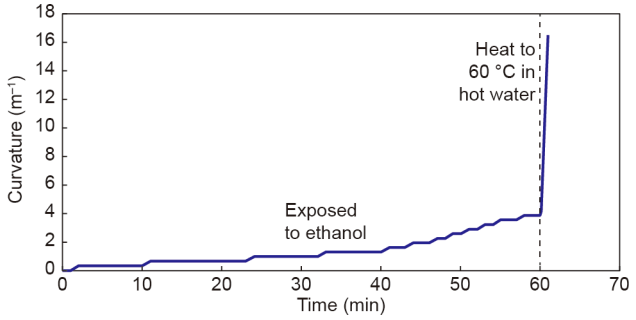

Fig. 12. 61 min response rate curve at 25 °C. The sample was exposed to ethanol for the first 60 min and then removed and heated in 60 °C hot water for the last minute.

The swelling of the TangoBlackPlus acted as the external force required to bend the bilayer. The swelling was able to produce a sufficient force to result some bending; however, the full potential of the curvature was not realized. After swelling the sample for 60 min—which was the time limit used for this study—and placing the sample in hot water, the sample started to bend more. It took a while to realize the curvature, as it did not occur immediately due to the heat transfer from the water to the VeroWhitePlus. A faster process could be achieved if direct heating were used.

The same situation is illustrated by Fig. 13; in this figure, the photos were taken at 10 min intervals when the sample was soaked in ethanol and at 10 s intervals during heating. These images tally with the curve shown in Fig. 12, in which there is little or close to no bending at the start. Fig. 13 also shows that during the course of swelling, the TangoBlackPlus visibly swelled up, while there was no change in the thickness of the VeroWhitePlus.

3.9. Repeatability

A sample with the same dimensions as the response rate test was used to study the repeatability of the reversibility cycle.

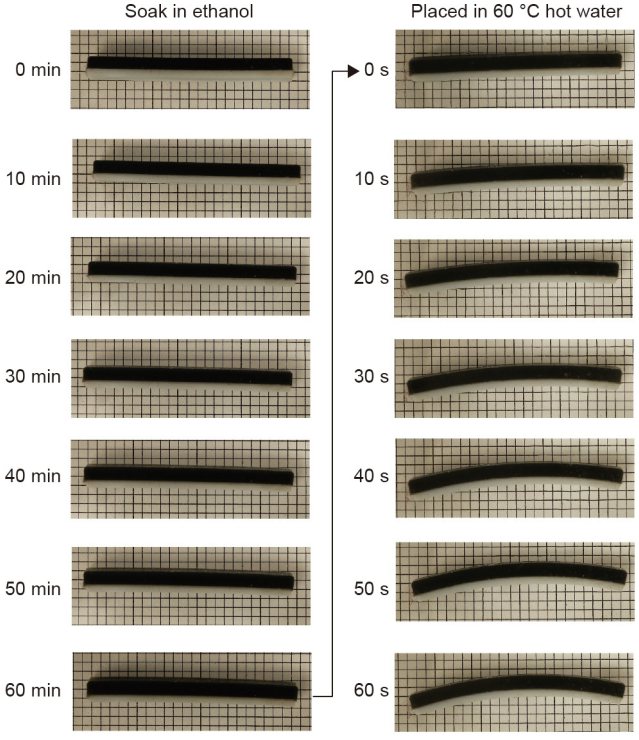

Fig. 13. First actuation cycle of the printed bilayer sample with a 1.5 mm thickness of VeroWhitePlus and a 2.5 mm thickness of TangoBlackPlus. The curvature is shown at intervals of 10 min for soaking in ethanol and at intervals of 10 s during heating.

Fig. 14 shows the photos taken after the programming and recovery stages. The steps were carried out as described for the demonstration of reversibility in Section 3.4. A clip was used to fix the end. The figure shows that after the first, second, or even fifth actuation, the amount of curvature remained similar. Also, after the

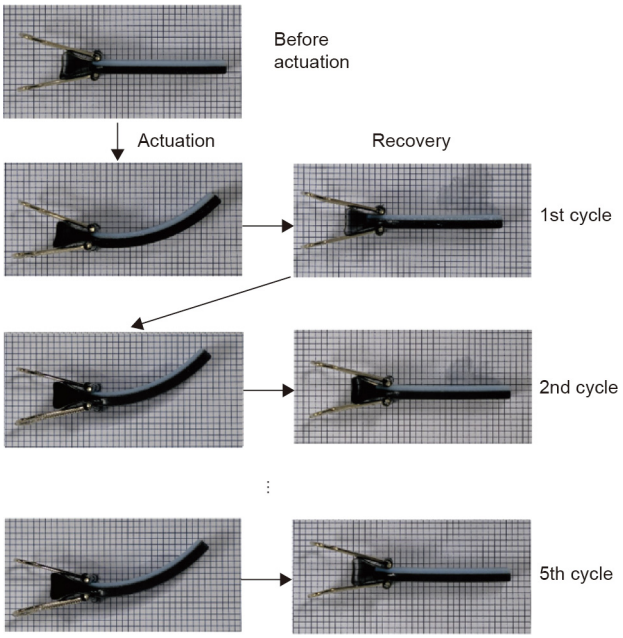

Fig. 14. Actuation results showing the actuation and recovery. The pre-actuated sample has a straight shape. After actuation, it curls up. In the recovery stage, it straightens again.

recovery stage, the sample was able to return to a straight shape. However, it is important to note that after multiple recoveries and up to ten repeated cycles, the VeroWhitePlus started to creep slightly when the structure was left to dry.

4. Conclusion

Complex structures with reversible shape changes will be revolutionary in many engineering applications such as building and construction, packaging and logistics [31], and biomedical applications such as food and drug delivery [32–35]. However, reversibility in 4D printing is currently still in its infancy. In this study, we proposed a simple dual-layer design to allow for a large amount of shape change. This study demonstrated the process of reversible 4D printing and verified that the use of a swellable elastomer is feasible for reducing the number of layers required in reversible 4D printing. Understanding the swelling behavior makes it possible to control the degree of swelling in the elastomer. In this case, the elastomer was TangoBlackPlus and the amount of swelling was temperature dependent. By coupling the swelling of the elastomer to the bilayer structure of a shape-setting polymer in a dual-layer structure, we were able to control the curvature using various parameters such as the temperature and the layer thickness of elastomer. Hence, the shape setting can be well-programmed. As a multi-material printer is required for such a design, in the current stage, we are limited to materials that are provided by Stratasys. In future, once more materials are available, it may be possible to use elastomers that can be swelled in other solvents, to enable real-life applications.

Acknowledgements

This research is supported by the Singapore Centre for 3D Printing, which is funded by the Singapore National Research Foundation.

Compliance with ethics guidelines

Amelia Yilin Lee, Jia An, Chee Kai Chua, and Yi Zhang declare that they have no conflict of interest or financial conflicts to disclose.

Appendix A. Supplementary data

Supplementary data to this article can be found online at https://doi.org/10.1016/j.eng.2019.09.007.

References

[1] Tibbits S. 4D printing: multi-material shape change. Archit Des 2014;84(1):116–21.
[2] Gardan J. Smart materials in additive manufacturing: state of the art and trends. Virtual Phys Prototyping 2019;14:1–18.
[3] Khoo ZX, Teoh JEM, Liu Y, Chua CK, Yang S, An J, et al. 3D printing of smart materials: a review on recent progresses in 4D printing. Virtual Phys Prototyping 2015;10(3):103–22.
[4] Chua CK, Leong KF. 3D printing and additive manufacturing: principles and applications—the 5th edition of rapid prototyping: principles and applications. Singapore: World Scientific Publishing Co Inc.; 2017.
[5] Lee AY, An J, Chua CK. Two-way 4D printing: a review on the reversibility of 3D-printed shape memory materials. Engineering 2017;3(5):663–74.
[6] Li J, Rodgers WR, Xie T. Semi-crystalline two-way shape memory elastomer. Polymer 2011;52(23):5320–5.
[7] Naficy S, Gately R, Gorkin R, Xin H, Spinks GM. 4D printing of reversible shape morphing hydrogel structures. Macromol Mater Eng 2017;302(1):1600212.
[8] Su JW, Tao X, Deng H, Zhang C, Jiang S, Lin Y, et al. 4D printing of a self-morphing polymer driven by a swellable guest medium. Soft Matter 2018;14(5):765–72.
[9] Huang L, Jiang R, Wu J, Song J, Bai H, Li B, et al. Ultrafast digital printing toward 4D shape changing materials. Adv Mater 2017;29(7):1605390.
[10] Mao Y, Ding Z, Yuan C, Ai S, Isakov M, Wu J, et al. 3D printed reversible shape changing components with stimuli responsive materials. Sci Rep 2016;6:24761.
[11] Ula SW, Traugutt NA, Volpe RH, Patel RR, Yu K, Yakacki CM. Liquid crystal elastomers: an introduction and review of emerging technologies. Liq Cryst Rev 2018;6:78–107.
[12] Wu X, Huang WM, Zhao Y, Ding Z, Tang C, Zhang J. Mechanisms of the shape memory effect in polymeric materials. Polymers 2013;5(4):1169–202.
[13] Ratna D, Karger-Kocsis J. Recent advances in shape memory polymers and composites: a review. J Mater Sci 2008;43(1):254–69.
[14] Treloar LRG. The elasticity and related properties of rubbers. Rep Prog Phys 1973;36(7):755–826.
[15] Qamar SZ, Akhtar M, Pervez T, Al-Kharusi MSM. Mechanical and structural behavior of a swelling elastomer under compressive loading. Mater Des 2013;45:487–96.
[16] Cai S, Lou Y, Ganguly P, Robisson A, Suo Z. Force generated by a swelling elastomer subject to constraint. J Appl Phys 2010;107(10):103535.
[17] Seehra MS, Yalamanchi M, Singh V. Structural characteristics and swelling mechanism of two commercial nitrile-butadiene elastomers in various fluids. Polym Test 2012;31(4):564–71.
[18] Dhaliwal JS, Negi MS, Kapur GS, Kant S. Compatibility studies on elastomers and polymers with ethanol blended gasoline. J Fuels 2014;2014:1–8.
[19] McCann MP. Physical chemistry CD (Laidler, Keith James; Meiser, John H.; Sanctuary, Bryan C.). J Chem Educ 2003;80(5):489.
[20] Kosiyanon R, McGregor R. Free volume theory of diffusion: method of predicting activation energies of diffusion for gases in elastomers. J Appl Polym Sci 1981;26(2):629–41.
[21] Ding Z, Yuan C, Peng X, Wang T, Qi HJ, Dunn ML. Direct 4D printing via active composite materials. Sci Adv 2017;3(4):e1602890.
[22] Fullcure material. Vero family [Internet]. Utah: GoEngineer; c2019 [cited 2019 Jan 31]. Available from: https://www.goengineer.com/products/vero-family/.
[23] Mettler-Toledo AG. Operating instructions: excellence balance XS models—part 2. Geifensee: Mettler-Toledo AG Laboratory & Weighing Technologies; 2010.
[24] Flory PJ, Rehner J Jr. Statistical mechanics of cross-linked polymer networks II. Swelling. J Chem Phys 1943;11(11):521–6.
[25] Fick A. On liquid diffusion. J Membr Sci 1995;100(1):33–8.
[26] Siepmann J, Podual K, Sriwongjanya M, Peppas NA, Bodmeier R. A new model describing the swelling and drug release kinetics from hydroxypropyl methylcellulose tablets. J Pharm Sci 1999;88(1):65–72.
[27] Orwoll RA, Arnold PA. Polymer–solvent interaction parameter. In: Mark JE, editor. Physical properties of polymers handbook. New York: Springer; 2007. p. 233–57.
[28] Utracki LA. Thermodynamics of polymer blends. In: Utracki LA, editor. Polymer blends handbook. Dordrech: Springer; 2003. p. 123–201.
[29] Czerner M, Fellay LS, Suárez MP, Frontini PM, Fasce LA. Determination of elastic modulus of gelatin gels by indentation experiments. Proc Mater Sci 2015;8:287–96.

[30] Teoh JEM, An J, Feng X, Zhao Y, Chua CK, Liu Y. Design and 4D printing of cross-folded origami structures: a preliminary investigation. Materials 2018;11(3):376.
[31] Ge Q, Dunn CK, Qi HJ, Dunn ML. Active origami by 4D printing. Smart Mater Struct 2014;23(9):094007.
[32] An J, Chua CK, Mironov V. A perspective on 4D bioprinting. Int J Bioprint 2016;2(1):3–5.
[33] Tan C, Toh WY, Wong G, Lin L. Extrusion-based 3D food printing—materials and machines. Int J Bioprinting 2018;4(2):143.
[34] Voon SL, An J, Wong G, Zhang Y, Chua CK. 3D food printing: a categorised review of inks and their development. Virtual Phys Prototyping 2019;14(3):203–18.
[35] Lepowsky E, Tasoglu S. 3D printing for drug manufacturing: a perspective on the future of pharmaceuticals. Int J Bioprint 2018;4(1):119.